Research Square

Preprints are preliminary reports that have not undergone peer review.
They should not be considered conclusive, used to inform clinical practice,
or referenced by the media as validated information.

Head-to-Head Preclinical Comparison of a Triazine-Based SSTR2 Homodimer and SSTR2/FAP Heterodimer in Neuroendocrine Tumors

Le Li

l.li.2@erasmusmc.nl

Erasmus Medical Centre: Erasmus MC

Hanyue Ma

Erasmus Medical Centre: Erasmus MC

Dylan Blijleven

Erasmus Medical Centre: Erasmus MC

Amber Piet

Erasmus Medical Centre: Erasmus MC

Corrina de Ridder

Erasmus Medical Centre: Erasmus MC

Debra Stuurman

Erasmus Medical Centre: Erasmus MC

Priciana Paraïso

Erasmus Medical Centre: Erasmus MC

Yann Seimbille

Erasmus Medical Centre: Erasmus MC

Research Article

Keywords: Neuroendocrine tumors, SSTR2, FAP, bivalent ligands, targeted radionuclide therapy

Posted Date: August 13th, 2026

DOI: https://doi.org/10.21203/rs.3.rs-10620672/v1

License: This work is licensed under a Creative Commons Attribution 4.0 International License.
Read Full License

Head-to-Head Preclinical Comparison of a Triazine-Based SSTR2 Homodimer and SSTR2/FAP Heterodimer in Neuroendocrine Tumors

Le Li[1,2 †], Hanyue Ma[1,2 †], Dylan Blijleven[1,2], Amber Piet[1,2], Corrina de Ridder[1,2], Debra Stuurman[1,2], Priciana Paraïso[1,2], Yann Seimbille[1,2 *]

1. Erasmus MC, University Medical Center Rotterdam, Department of Radiology and Nuclear Medicine, Rotterdam, The Netherlands
2. Erasmus MC Cancer Institute, Rotterdam, The Netherlands

† These authors contributed equally to this work.

***** Correspondence: y.seimbille@erasmusmc.nl; Tel: +31 10-703-8961

Abstract:

Objective: To compare the tumor targeting and pharmacokinetic properties of a SSTR2 (somatostatin receptor type 2) homodimer **8** and a SSTR2/FAP (fibroblast activation protein) heterodimer **14** for neuroendocrine tumors.

Methods: Both dimers were synthesized on a modular triazine platform with PEG_2 linkers and labeled with lutetium-177. Radiochemical purity, lipophilicity, receptor affinity, and cellular uptake were evaluated. *Ex vivo* biodistribution studies were conducted in H69 tumor-bearing mice at 1, 4, and 24 h post-injection (p.i.). Autoradiography and immunohistochemistry were performed on tumor sections.

Results: Both dimers showed high radiochemical purity (>95%), good stability, and SSTR2 affinity similar to DOTA-TATE. The heterodimer **14** showed approximately 2-fold higher uptake in FAP-positive cells than [^{177}Lu]Lu-FAPI-46. In H69 xenografts, both dimers demonstrated comparable tumor exposure ($AUC_{0\text{-}24\ h}$ = 98.21 ± 5.45 vs. 97.89 ± 3.50) and retention kinetics ($t_{1/2}$ = 12.6 h vs. 12.9 h). Compared with homodimer **8**, heterodimer **14** exhibited favorable pharmacokinetics, including reduced renal uptake and prolonged blood circulation. Under SSTR2 blockade, heterodimer **14** retained partial tumor uptake, suggesting additional non-SSTR2-mediated interactions. Autoradiography demonstrated the blockade-resistant uptake of [^{177}Lu]Lu-**14**, and immunohistochemistry confirmed FAP expression in H69 tumors.

Conclusion: Both dimers achieved effective SSTR2-mediated tumor targeting. Compared with homodimer **8**, heterodimer **14** exhibited distinct pharmacokinetic characteristics while maintaining comparable tumor targeting, supporting the feasibility of SSTR2/FAP dual-targeting.

Keywords: Neuroendocrine tumors; SSTR2; FAP; bivalent ligands; targeted radionuclide therapy.

1 Introduction

Neuroendocrine tumors (NETs) comprise a biologically heterogeneous group of malignancies arising from neuroendocrine cells and characterized by marked variability in receptor expression, growth kinetics, and clinical behavior (1, 2). This heterogeneity results in diverse clinical presentations and complicates therapeutic management (3-5). Conventional treatment strategies include surgery, somatostatin analogs (SSAs), chemotherapy, targeted therapies, and liver-directed interventions (6, 7).

Peptide receptor radionuclide therapy (PRRT) has recently emerged as an important treatment option for patients with advanced inoperable NETs expressing somatostatin receptors (SSTRs) (2, 8, 9). Among the five known SSTR subtypes (SSTR1-5), SSTR2 is the predominant isoform in well-differentiated NETs and represents the principal molecular target for current radiopharmaceuticals (10). Radiotracers, such as [^{68}Ga]Ga-DOTA-TATE and [^{64}Cu]Cu-DOTA-TATE, have substantially improved imaging, staging, and patient stratification, while [^{177}Lu]Lu-DOTA-TATE (Lutathera®) has demonstrated significant therapeutic benefit by delivering targeted radiation to SSTR-positive tumors (11-14).

However, therapeutic efficacy remains limited in a subset of patients, particularly those with high-grade or poorly differentiated NETs that exhibit low or heterogeneous SSTR2 expression. The insufficient radioligand uptake in these cases highlights the need for alternative molecular design strategies capable of overcoming receptor heterogeneity or low SSTR2 expression (15). One promising approach is peptide dimerization, which can enhance binding avidity, metabolic stability, circulation time, and tumor retention through multivalent interactions (16). Homodimeric constructs targeting SSTR2 can increase binding avidity when receptor density is sufficient, leading to enhanced tumor uptake and prolonged tumor retention without altering biological specificity (17).

In parallel, heterodimeric radioligands capable of targeting two biomarkers simultaneously offer a complementary strategy (18, 19). Fibroblast activation protein (FAP), expressed on cancer-associated fibroblasts and frequently upregulated in aggressive NET phenotypes with reduced SSTR2 expression, represents a particularly relevant secondary target (20-22). FAP-directed small-molecule radiotracers, including [^{68}Ga]Ga-FAPI-46 and [^{68}Ga]Ga-OncoFAP, exhibit rapid tumor accumulation and high imaging contrast, although their short tumor retention limits therapeutic applicability (23-25).

Building on our previous development of the dual-targeting ligand eSOMA-FAP-02 (unpublished data), a first-generation heterodimer designed for simultaneous targeting of SSTR2 and FAP, we established the feasibility of dual-receptor targeting *in vivo*. However, although proof-of-concept was achieved, eSOMA-FAP-02 exhibited suboptimal pharmacokinetics, resulting in insufficient tumor-to-background ratio. This encouraged us to optimize the molecular architecture to improve tumor targeting efficacy and overall *in vivo* performance. The present study extends this approach by synthesizing and evaluating a next-generation SSTR2-targeting homodimer **8** and SSTR2/FAP-targeting heterodimer **14** (Fig. 1). These constructs were assembled using a triazine-based platform incorporating TATE-derived SSTR2-targeting units, a FAP-targeting motif, and the 1,4,7,10-tetraazacyclododecane-1-

glutaric anhydride-4,7,10-triacetic acid (DOTA-GA) chelator to generate homodimeric and heterodimeric radioligands. Ultimately, **8** and **14** could improve targeting of high-grade or poorly differentiated NETs with low or heterogeneous SSTR2 expression. Using a shared molecular framework to isolate the effects of valency and target multiplicity, this study systematically compared homodimeric and heterodimeric radioligands. The aim was to elucidate the role of dimerization and dual-targeting on hydrophilicity, stability, and receptor binding, and to assess their respective impact on tumor uptake, retention, and biodistribution in neuroendocrine tumor models.

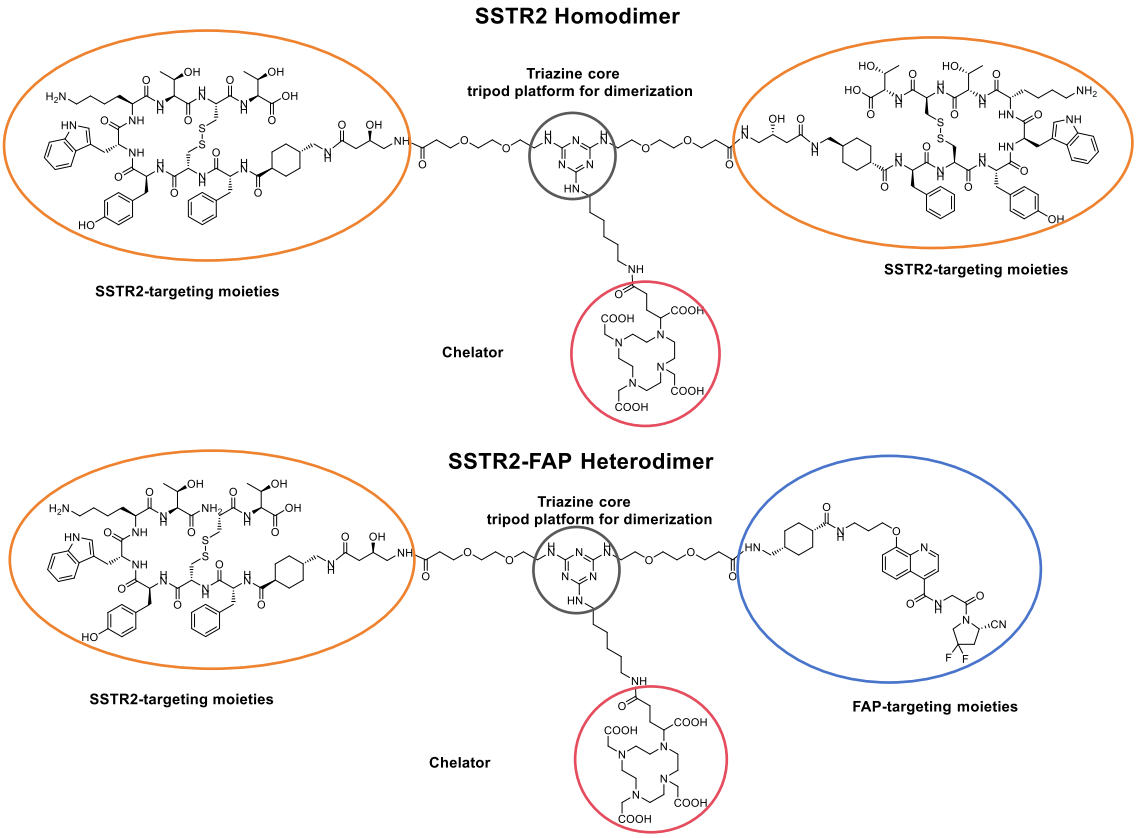


Figure 1. *Chemical structures of the SSTR2-targeting homodimer* ***8*** *and SSTR2/FAP-targeting heterodimer* ***14.*** *The dimers were constructed on a triazine-based scaffold (in gray) enabling modular conjugation of the SSTR2-targeting cyclic peptide derived from TATE (in orange), the FAP-targeting unit based on 8-QCP (in blue), and the DOTA-GA chelator (in red).*

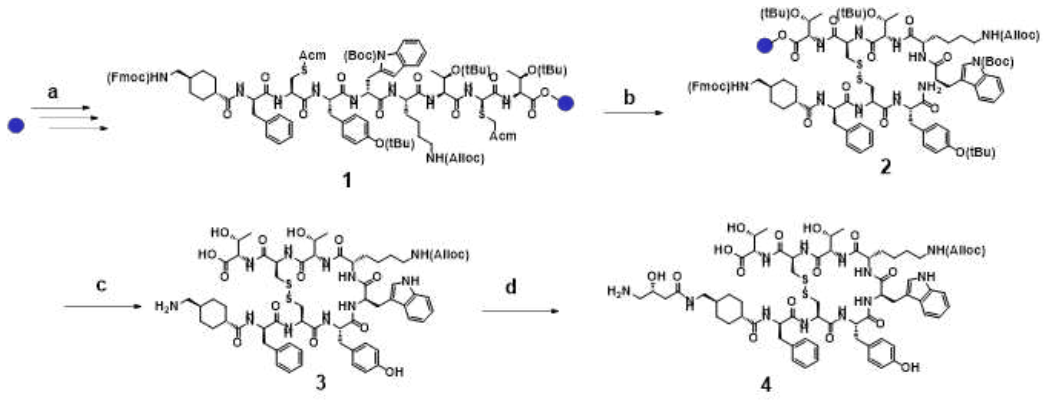
2 Results

2.1 Chemistry

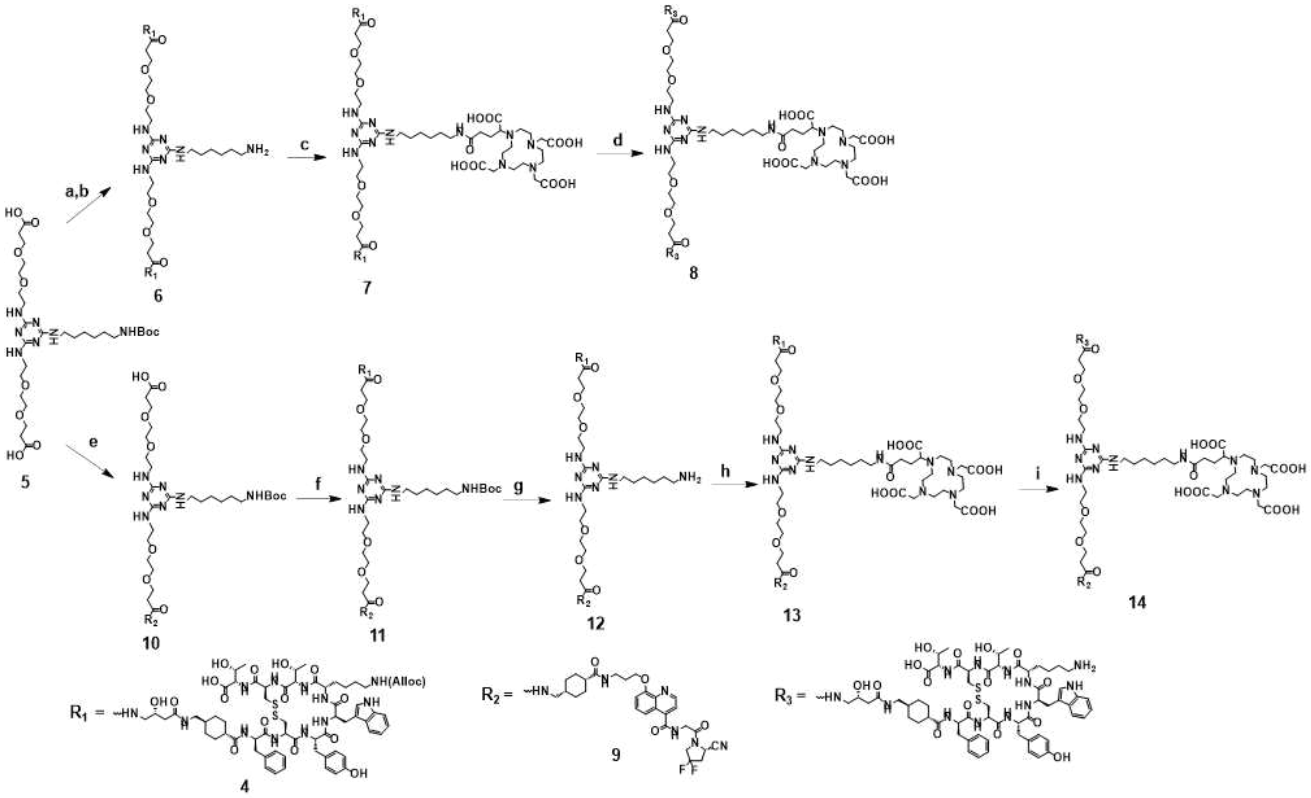
The SSTR2 binding peptide **3** (26) and FAP binding unit **9** (27) were selected from libraries previously developed in our group. The cyclic peptide **3** was synthesized via standard Fmoc-based solid-phase peptide synthesis (SPPS) (Scheme 1). To increase peptide hydrophilicity, a GABOB linker was introduced, yielding compound **4** in 46% yield. The synthesis of both dimers was achieved using a PEG_2-functionalized 1,3,5-triazine core **5** previously developed in our laboratory (28) as a modular platform for multivalent ligand assembly (Scheme 2).

The SSTR2-targeting homodimer **8** was prepared by conjugation of two SSTR2-targeting peptides **4** to the triazine-based platform **5,** followed by Boc removal with TFA to afford the corresponding amine **6** in 28% yield. Subsequent coupling of **6** with the chelating agent DOTA-GA anhydride, afforded the intermediate **7** in 81% yield. Final Alloc deprotection afforded **8** in 50% yield with >95% chemical purity, as confirmed by LC-MS (Fig. S5).

Synthesis of the SSTR2/FAP-targeting heterodimer **14** consisted of conjugation of the SSTR2-targeted peptide **4** to the triazine platform **5** to afford monosubstituted intermediate **10** in 26% yield, followed by the attachment of FAP-targeting moiety **9** to give **11** in 50% yield. Following Boc deprotection, the corresponding amine **12** was coupled with DOTA-GA anhydride to afford intermediate **13** in 47% yield over two steps. Final Alloc deprotection gave the desired heterodimer **14** in 36% yield with >95% chemical purity (Fig. S10).



Scheme 1: *Synthesis of the GABOB-functionalized cyclic peptide **4**. Reagents and conditions: (a) Fmoc-SPPS; (b) TTFA, DMF, rt, 3 h; (c) 20% piperidine in DMF, rt, 15 min; (d) TFA/DCM/TIPS (95:2.5:2.5, v/v/v), rt, 3 h, 50%; (e) Boc-GABOB-OH, HBTU, DIPEA, DMF, rt, 1 h; (f) TFA/DCM (1:1, v/v), rt, 30 min, 46%, over two steps.*



Scheme 2. *Chemical syntheses of the SSTR2 homodimer **8** and SSTR2/FAP heterodimer **14**. Reagents and conditions: (a) **4**, DMF, HBTU, DIPEA, rt, 1 h; (b) TFA/DCM/TIPS (95:2.5:2.5, v/v/v), rt, 30 min, 28% over two steps; (c) DOTA-GA anhydride, DMF, DIPEA, rt, 1 h, 81%; (d) $Pd(PPh_3)_4$, $PhSiH_3$, DCM, rt, 3 h, 50%; (e) **9**, DMF, HBTU, DIPEA, rt, 1 h, 26%; (f) **4**, DMF, HBTU, DIPEA, rt, 1 h, 50%; (g) TFA/DCM (1:1, v/v), rt, 30 min, 74%; (h) DOTA-GA anhydride, DMF, DIPEA, rt, 1 h, 64%; (i) $Pd(PPh_3)_4$,$PhSiH_3$, DCM, rt, 3 h, 36%.*

2.2 Radiochemistry, stability and lipophilicity

The two dimers were efficiently radiolabeled with lutetium-177, achieving radiochemical yields (RCY) and radiochemical purities (RCP) above 95% (Table 1, Fig. S11-12). The stability of [^{177}Lu]Lu-**8** and [^{177}Lu]Lu-**14** was assessed by radio-HPLC after incubation in phosphate-buffered saline (PBS) and murine serum for 1, 4, and 24 h. Both radiotracers demonstrated high stability in PBS, with radiochemical purities remaining > 88% after 24 h. In murine serum, [^{177}Lu]Lu-**8** showed relatively higher stability, retaining > 89% intact compound at 24 h, whereas [^{177}Lu]Lu-**14** exhibited moderate degradation, with 78% intact tracer remaining at 24 h post-incubation. The lipophilicity of both compounds was determined by $LogD_{7.4}$ measurements (Table 1). Both dimers were highly hydrophilic, as demonstrated by the negative $LogD_{7.4}$ values (-1.8 ± 0.1 and -2.1 ± 0.1 for [^{177}Lu]Lu-**8** and [^{177}Lu]Lu-**14**, respectively).

Table 1. *Radiochemical proprieties of [^{177}Lu]Lu-**8** and [^{177}Lu]Lu-**14**.*

Compound	RCY (%)	RCP (%)	$LogD_{7.4}$ (n=3)	PBS (%)*			Murine serum (%)*		
				1 h	4 h	24 h	1 h	4 h	24 h
[^{177}Lu]Lu-**8**	> 95	99.7	-1.8 ± 0.1	96.5	94.5	94.3	96.1	89.7	89.5
[^{177}Lu]Lu-**14**	> 95	95.3	-2.1 ± 0.1	93.1	90.8	88.9	92.0	88.9	78.4

* Results are expressed as the percentage of intact labeled ligand after incubation at 37 °C (n = 1)

2.3 Binding affinity for SSTR2, huFAP, muFAP, and DPP4

Competitive binding assay was carried out in U2OS.SSTR2 cells and [^{177}Lu]Lu-DOTA-TATE was used as a radioligand (Fig. 2). Both dimers exhibited IC_{50} values for SSTR2 comparable to DOTA-TATE (5.3 ± 0.3 nM, 8.8 ± 0.8 nM and 6.0 ± 1.7 nM for DOTA-TATE, compounds **8** and **14**, respectively), confirming high receptor binding affinity. The affinity of **14** for human FAP (huFAP), murine FAP (muFAP), and the related protease DPP4 was determined using a recombinant enzymatic assay (Table 2). The heterodimer **14** exhibited nanomolar IC_{50} values for huFAP and muFAP, while showing markedly lower affinity for DPP4, demonstrating high selectivity for FAP over DPP4.

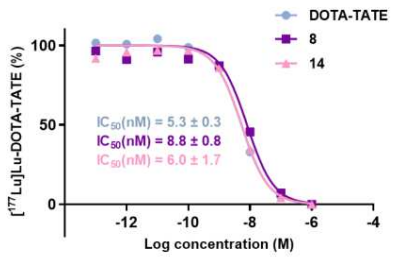


Figure. 2*. Competitive binding assay on U2OS.SSTR2 cells and corresponding IC_{50} values of DOTA-TATE,* ***8*** *and* ***14*** *(n = 3).*

Table 2. *IC_{50} values of the SSTR2/FAP-targeting heterodimer* ***14*** *for huFAP, muFAP and DPP4.*

Compound	Inhibition		Specificity
	$IC_{50,\ huFAP}$ nM	$IC_{50,\ muFAP}$ nM	$IC_{50,\ DPP4}$ µM
FAPI-46	1.5± 0.5	1.4 ± 0.5	20.5 ± 2.5
14	2.9 ± 0.5	2.0 ± 0.3	n.d.

n.d.: not determined due to insufficient inhibition for reliable curve fitting.

2.4 Cell uptake and binding studies

Uptake and internalization of the two dimers were investigated in U2OS.SSTR2 and HT-1080.huFAP cell lines (Fig. 3). In U2OS.SSTR2 cells, the uptakes of [^{177}Lu]Lu-**8** and [^{177}Lu]Lu-**14** were lower than the reference [^{177}Lu]Lu-DOTA-TATE (25.2 ± 6.5% AD at 0.5 h and 61.4 ± 6.4% AD at 2 h). The uptake of [^{177}Lu]Lu-**8** increased from 22.7 ± 4.1% AD at 0.5 h to 49.2 ± 3.2% AD at 2 h, similarly, the uptake of [^{177}Lu]Lu-**14** showed an increase from 15.4 ± 5.1% AD to 41.6 ± 3.3% AD within 2h (Fig. 3A). In HT-1080.huFAP cells, [^{177}Lu]Lu-**14** displayed a greater increase in uptake overtime, reaching 37.0 ± 6.4% AD at 2h, approximately 2-fold higher than that of the reference [^{177}Lu]Lu-FAPI-46 (17.6 ± 4.3% AD) (Fig. 3B). As expected, high internalization (>90% of the total uptake) was observed for [^{177}Lu]Lu-**8** in U2OS.SSTR2 cells and [^{177}Lu]Lu-**14** in both cell lines (Fig. 3A & 3B). The uptake specificity was confirmed by co-incubation with an excess of unlabeled DOTA-TATE or FAPI-46, which resulted in negligible uptake for all radiotracers (Table S1).

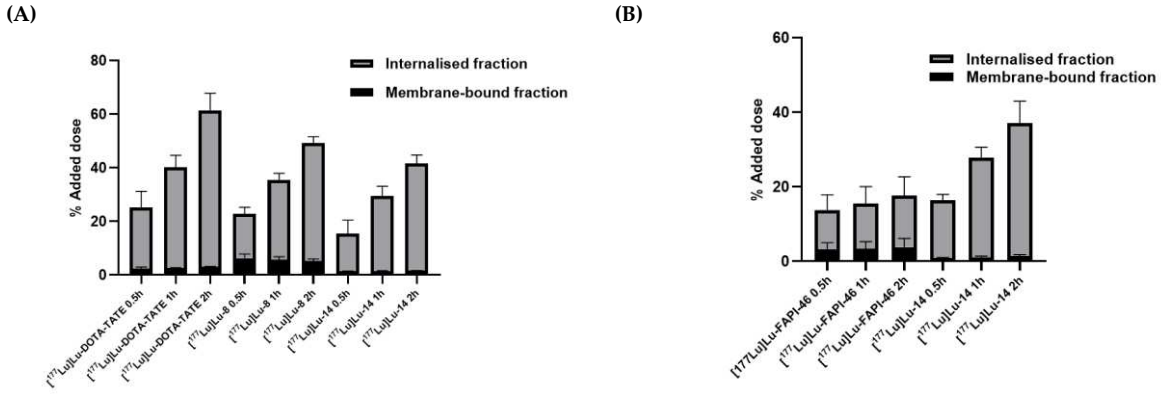


Figure. 3*. Cell uptake and internalization studies of [^{177}Lu]Lu-DOTA-TATE, [^{177}Lu]Lu-**8**, and [^{177}Lu]Lu-**14** using U2OS.SSTR2 (A) and HT-1080.huFAP cells (B) at different time points.*

2.5 *Ex vivo* biodistribution

Ex vivo biodistribution studies were carried out at 1, 4, and 24 h after administration of [^{177}Lu]Lu-**8** and [^{177}Lu]Lu-**14**. An additional group of mice was co-injected with a 100-fold molar excess of unlabeled DOTA-TATE and sacrificed at 4 h post-injection (p.i.) (4 h-block group) to evaluate SSTR2-targeted uptake specificity (Fig. 4, Table S2 & S3). Pharmacokinetic analysis was performed to determine the biological half-life ($t_{1/2}$) and tissue exposure ($AUC_{0 \rightarrow 24\ h}$) of tumors, blood, and major organs (Fig. 5).

Both radiotracers demonstrated comparable tumor uptake at early time points, reaching 5.76 ± 0.80% ID/g for [^{177}Lu]Lu-**8** and 5.66 ± 0.97% ID/g for [^{177}Lu]Lu-**14** at 1 h p.i. Tumor uptake gradually decreased at 4 h and 24 h p.i., resulting in comparable tumor half-lives (12.6 h for [^{177}Lu]Lu-**8** and 12.9 h for [^{177}Lu]Lu-**14)** and overall tumor exposure ($AUC_{0 \rightarrow 24\ h}$: 98.21 ± 5.45 and 97.89 ± 3.50, respectively). Blocking with excess unlabeled DOTA-TATE markedly reduced tumor and pancreas uptake at 4 h p.i. of [^{177}Lu]Lu-**8** (tumor: 0.59 ± 0.03% ID/g vs. 4.96 ± 0.59% ID/g; pancreas: 0.30 ± 0.02% ID/g vs. 2.74 ± 0.57% ID/g), confirming SSTR2-specific tracer accumulation. However, only a moderate reduction in tumor uptake (3.23 ± 0.70% ID/g vs. 5.07 ± 0.27% ID/g) and no significant change in pancreatic uptake (2.02 ± 0.20% ID/g vs. 2.21 ± 0.24% ID/g) were observed following co-administration of DOTA-TATE with [^{177}Lu]Lu-**14**. These findings indicate that the accumulation of [^{177}Lu]Lu-**14** on tissues was not solely mediated by SSTR2. Consistently, higher uptake in the pancreas was observed for [^{177}Lu]Lu-**8** than [^{177}Lu]Lu-**14** (6.60 ± 1.46% ID/g vs. 4.16 ± 0.53% ID/g).

Renal uptake was markedly higher for the homodimer [^{177}Lu]Lu-**8**, reaching 107.3 ± 9.7% ID/g and 116.0 ± 4.6% ID/g at 1 and 4 h p.i., whereas [^{177}Lu]Lu-**14** showed substantially lower kidney retention (22.3 ± 2.4% ID/g at 1 h and 19.5 ± 1.6% ID/g at 4 h p.i., $p < 0.001$). Co-injection of excess unlabeled DOTA-TATE did not significantly reduce renal uptake for either tracer.

The heterodimer [^{177}Lu]Lu-**14** also exhibited a longer blood half-life than the homodimer (2.3 h vs. 1.0 h), resulting in higher blood pool activity at early time points. This prolonged circulation enhanced exposure in vascularized organs such as the liver, heart, and spleen, where uptake was significantly greater at 4 h p.i. compared to the homodimer ($p < 0.01$). Interestingly, the heterodimer [^{177}Lu]Lu-**14** also demonstrated high bone uptake at 1 h p.i.

(6.31 ± 1.08% ID/g), while bone uptake was nearly negligible for the homodimer [^{177}Lu]Lu-**8** (1.00 ± 0.40% ID/g), likely reflecting the contribution of the FAP targeting moiety in the structure of **14**. Additionally, [^{177}Lu]Lu-**14** showed significantly higher skin uptake compared to the [^{177}Lu]Lu-**8** (7.05 ± 0.73% ID/g at 1 h p.i. and 4.10 ± 0.35% ID/g at 4 h p.i. vs. 1.98 ± 0.27% ID/g at 1 h p.i. and 0.71 ± 0.04% ID/g at 4 h p.i., respectively, $p < 0.001$). Both radiotracers showed low background activity in most organs at 24 h p.i., reflecting efficient clearance from non-target tissues.

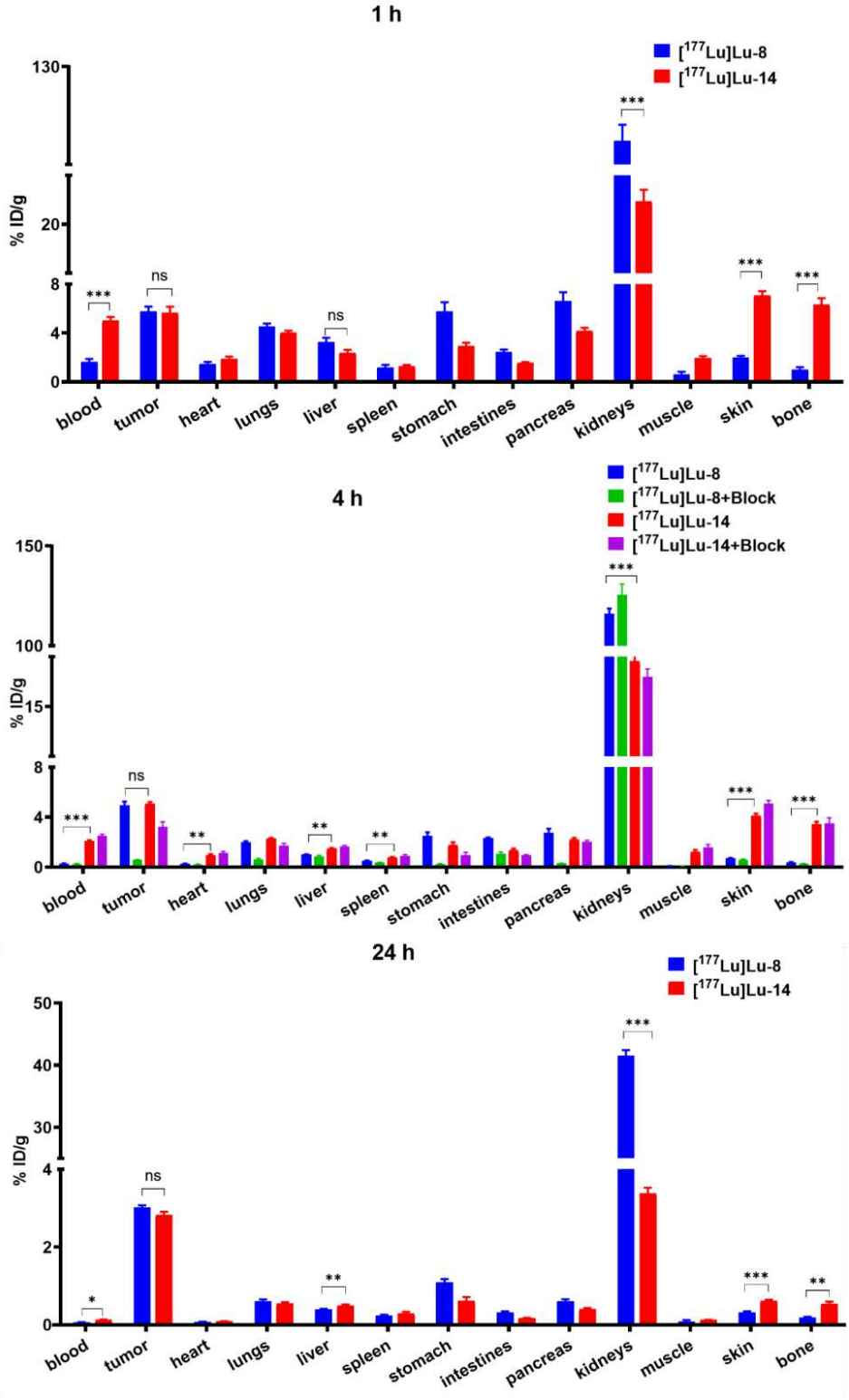


Figure 4. *Ex vivo biodistribution of [^{177}Lu]Lu-**8** and [^{177}Lu]Lu-**14** in H69 tumor bearing mice at 1, 4, and 24 h p.i.; A blocking group (4 h-block, co-injected with excess DOTA-TATE) was included for comparison. Uptake in tissues is expressed as the percentage of the injected dose per gram of tissue (% ID/g). Statistical significance between the two groups was determined using unpaired two-tailed Student's t-tests; *P < 0.05, **P < 0.01, *** P < 0.001, ns, not significant.*

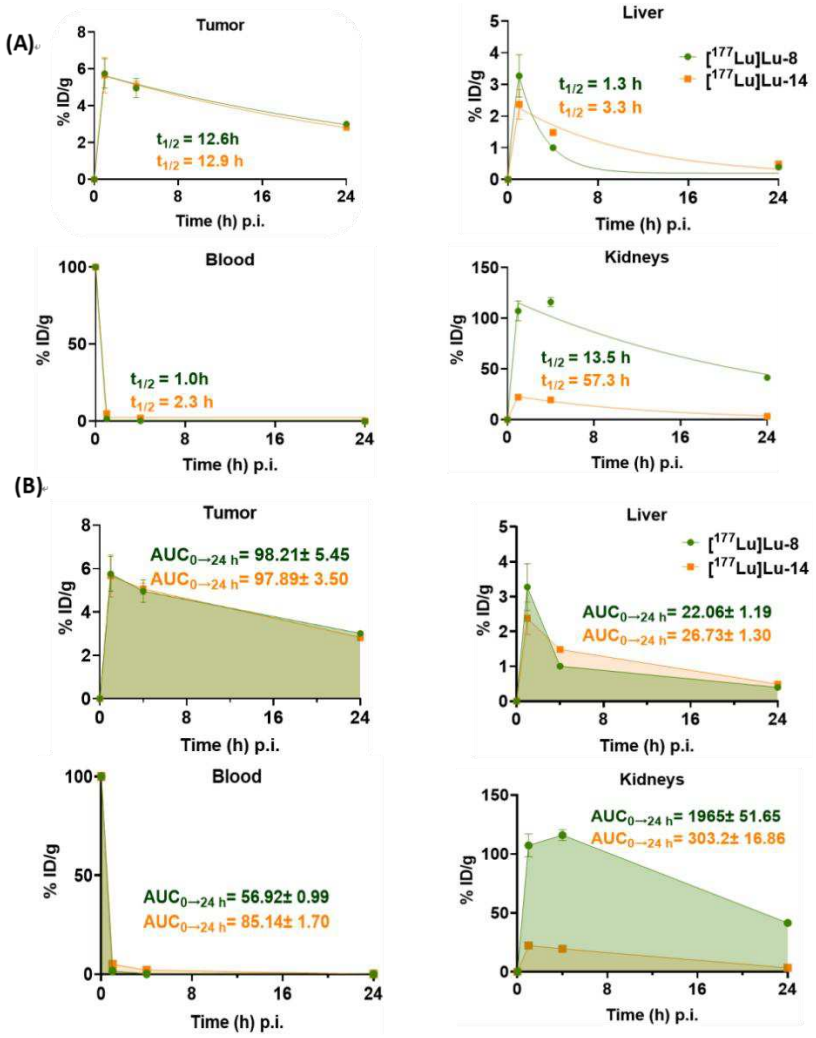


Figure 5. *(A) Pharmacokinetic modeling of major organs clearance for [^{177}Lu]Lu-**8** and [^{177}Lu]Lu-**14**. (B) Area under the curve up to 24 h p.i. ($AUC_{0 \rightarrow 24\,h}$) from the biodistribution data.*

2.6 Autoradiography studies

Ex vivo autoradiography of H69 tumor sections collected at 4 h post-injection revealed a broadly comparable and relatively even distribution of [^{177}Lu]Lu-**8** and [^{177}Lu]Lu-**14** across tumor sections under non-blocking conditions (Fig. 6). Under SSTR2 blockade, the autoradiographic signal of [^{177}Lu]Lu-**8** was markedly reduced from 1.7% to 0.5% AA (a 70.6% decrease), indicating predominantly SSTR2-mediated uptake. In contrast, [^{177}Lu]Lu-**14** retained a considerable residual signal under blocking conditions (from 2.3% to 1.1% AA, 48% of the activity measured under non-blocking conditions), suggesting the presence of an additional non-SSTR2-mediated uptake component. These findings are consistent with the quantitative *ex vivo* biodistribution results (Fig. 4).

To assess the contribution of FAP expression in the H69 tumor model used in this study, additional *in vitro* autoradiography using [^{111}In]In-FAPI-46 was performed on H69 tumor sections, with HT-1080.huFAP tumor sections serving as a FAP-positive control. H69 sections exhibited a detectable signal (4.3% AA, Fig. 7), whereas HT-1080.huFAP sections showed

substantially higher binding signal (42.3% AA, Fig. S13), approximately 10-fold greater than that observed in H69 sections.

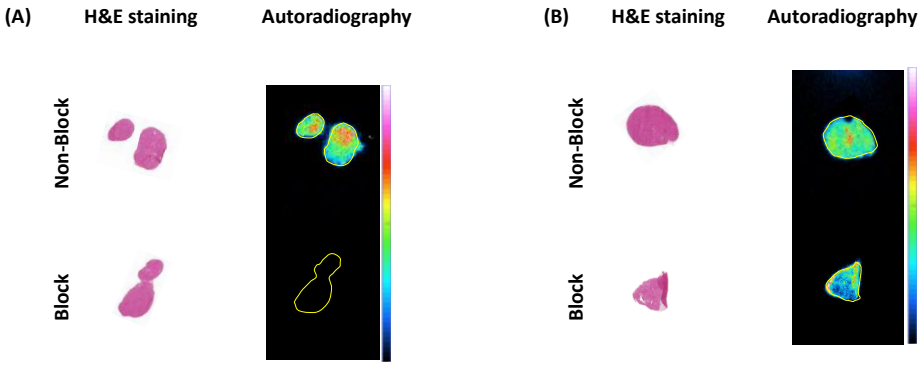


Figure 6. *Ex vivo autoradiography of H69 tumor sections at 4 h post-injection. Representative H&E-stained sections and corresponding autoradiograms are shown for [^{177}Lu]Lu-**8** (A) and [^{177}Lu]Lu-**14** (B) under non-blocked and blocked conditions.*

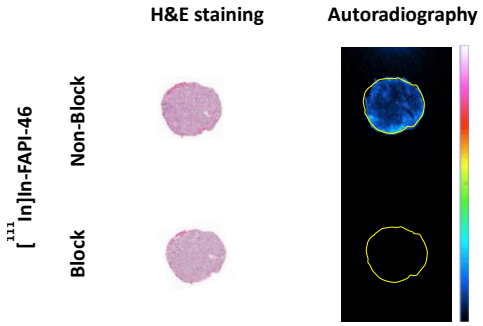


Figure 7. *In vitro autoradiography of H69 tumor sections. Representative H&E-stained sections and corresponding autoradiography are shown for [^{111}In]In-FAPI-46 under non-blocked and blocked conditions.*

2.7 Immunohistochemical validation

To confirm the presence of FAP, immunohistochemical staining for FAP was performed on H69 tumor sections, using HT-1080.huFAP xenografts as a positive control and FAP-negative tissue as a negative control (Fig. 8). Immunohistochemical analysis revealed distinct FAP distribution patterns in the FAP-positive specimens. In HT-1080.huFAP xenografts, FAP staining appeared as a homogeneous and diffuse pattern throughout the cell mass. In contrast, FAP immunoreactivity in H69 tumor xenografts was extensive throughout the tissue sections but displayed a fibrillar, bundle-like texture. The negative control tissue exhibited no specific immunoreactivity, confirming the specificity of the antibody.

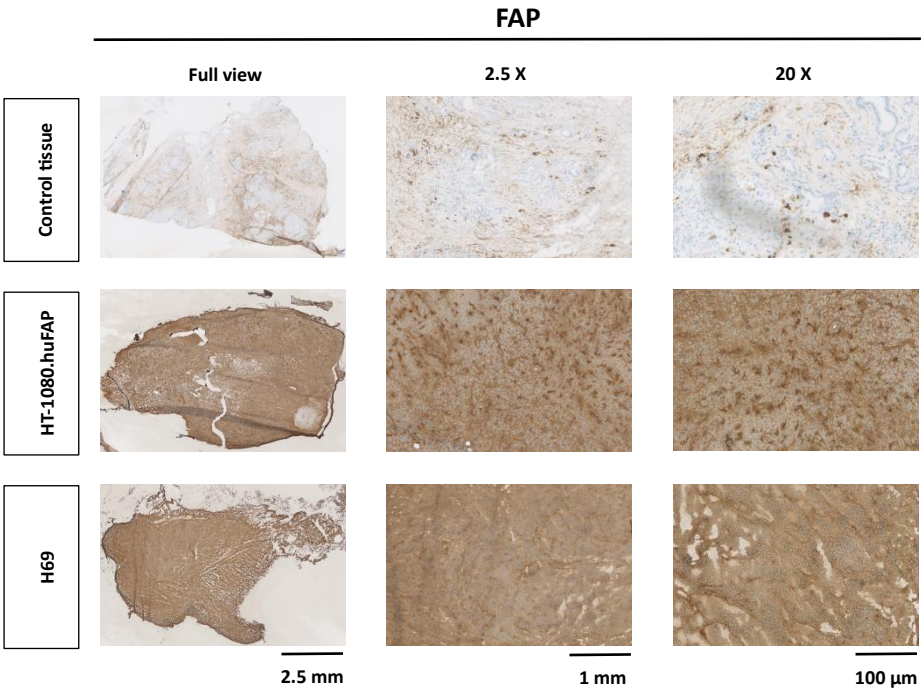


Figure 8. IHC assessment of FAP expression in FAP-negative control tissue, HT-1080.huFAP positive-control and H69 xenografts (full view/ 2.5x/ 20x). FAP immunoreactivity was visualized using DAB chromogen and appears brown, whereas nuclei were counterstained with hematoxylin.

3 Discussion

In this study, we successfully developed an SSTR2-targeting homodimer **8** and an SSTR2/FAP-targeting heterodimer **14** using a modular PEG_2-functionalized 1,3,5-triazine scaffold, previously developed in our group for multivalent ligand assembly (28). This platform enabled controlled sequential conjugation and structural symmetry, distinguishing it from previously reported PEG- or lysine-based SSTR2 dimers (19, 29). Both dimers were labeled with ^{177}Lu in high radiochemical yield and purity, and showed a hydrophilic character comparable to [^{177}Lu]Lu-DOTA-TATE ($LogD_{7.4}$ = -1.94 ± 0.01) (30). The heterodimer **14** retained binding affinity to FAP and SSTR2, with IC_{50} values in the nanomolar range. Serum stability was slightly lower for the heterodimer **14** compared to the homodimer **8** (78% vs. 89.5% intact radiotracer at 24 h), consistent with previous reports on peptide-small molecule heterodimers where conjugation may slightly affect stability without compromising receptor binding (31, 32).

The *in vitro* cell uptake and internalization studies confirmed that both dimers maintained high receptor specificity and efficient internalization. In U2OS.SSTR2 cells, high SSTR2-targeted uptake (40%-60% of added activity) was observed for both constructs, supporting their suitability for radionuclide therapy applications. In HT-1080.huFAP cells, [^{177}Lu]Lu-**14** demonstrated higher uptake than [^{177}Lu]Lu-FAPI-46, suggesting preserved functionality of the FAP-binding motif in a dual-targeting format. These *in vitro* findings provided the rationale for subsequent *in vivo* evaluation of both dimers.

Ex vivo biodistribution demonstrated comparable tumor uptake and exposure of both dimers in SSTR2-overexpressing xenografts. The Lu-177 labeled homodimer **8** showed a tumor uptake profile comparable to that of [^{111}In]In-DOTA-TATE previously reported by our group in the same H69 xenograft model (33). This lack of enhanced tumor uptake may reflect suboptimal molecular architecture, such as linker length, global charge, or spatial orientation, which could limit simultaneous engagement of adjacent SSTR2 receptors. Alternatively, agonist-induced dissociation of SSTR2 receptor homodimers has been proposed to be required for receptor internalization, a process that could be hindered by bivalent ligands (34, 35). Similarly, the heterodimer **14** maintained effective tumor targeting but did not show the enhanced tumor uptake reported for some SSTR2/FAP dual-targeting radiotracers (19, 29). This is consistent with the minimal FAP availability in H69 tumors, as confirmed by [^{111}In]In-FAPI-46 autoradiography, where the signal of [^{111}In]In-FAPI-46 was approximately 10-fold lower than in FAP-positive controls, thereby limiting the contribution of the FAP-targeting moiety to tumor accumulation. Immunohistochemical analysis further revealed a fibrillar FAP staining pattern in H69 tumors, suggestive of stromal CAF expression. This is consistent with the established role of FAP as a CAF marker (36) and with the known ability of tumor cells to recruit and convert host fibroblasts into CAFs during xenograft establishment (37, 38). High renal uptake of the homodimer **8** was expected for DOTA-TATE-based peptides, as kidneys represent the dose-limiting organ in peptide receptor radionuclide therapy due to proximal tubular reabsorption of radiolabeled somatostatin analogs (39, 40). Reduced kidney retention of the heterodimer **14** suggests that architectural modification significantly influences renal handling, as similarly observed in other heterobivalent peptide systems (41).

Notably, elevated bone uptake was observed exclusively for the heterodimer **14**. This is in line with previous reports showing bone accumulation in mice for other FAP-targeting radioligands (42, 43). However, such skeletal accumulation has not been consistently reported in previously described SSTR2/FAP heterodimers (19, 29), suggesting that this observation may be influenced by construct-specific properties. Importantly, this physiological bone uptake has not been reported in human FAPI PET/CT imaging (44, 45), suggesting that the murine bone accumulation is unlikely to affect its therapeutic potential. The heterodimer **14** also demonstrated prolonged blood circulation and delayed clearance. This extended circulation did not translate into enhanced tumor uptake, likely due to limited FAP availability in the H69 xenograft model. This pharmacokinetic feature may prove advantageous in tumors with a more prominent FAP-positive stromal compartment by providing greater opportunity for FAP engagement, thereby potentially improving tumor uptake and prolonging tumor exposure window (19, 29).

Nevertheless, although IHC confirmed the presence of FAP protein in H69 tumors, the current tumor model does not allow us to quantitatively distinguish SSTR2-mediated from FAP-mediated uptake *in vivo*. Consequently, the mechanistic basis of tumor accumulation remains incompletely defined, and the added value of dual-targeting cannot be fully established. Future studies in models with differential target expression, particularly those with sufficient FAP and SSTR2 co-expression, will be required to fully evaluate the potential of this heterodimeric strategy.

4 Conclusion

Both dimers demonstrated effective SSTR2-mediated tumor targeting *in vitro* and in H69 xenografts. Compared with the homodimer **8**, the SSTR2/FAP-targeting heterodimer **14** exhibited distinct *in vivo* pharmacokinetics, including altered tissue distribution and prolonged circulation. These findings indicate that SSTR2/FAP heterodimerization can modulate pharmacokinetic properties while preserving effective SSTR2-mediated tumor targeting. However, the contribution of FAP-mediated uptake remains to be elucidated in more clinically relevant tumor models with abundant FAP-positive stroma.

5 Materials and Methods

5.1 General information

5.1.1 Chemistry

All chemicals and solvents were obtained from commercial suppliers and used as received, unless otherwise specified. LC-MS was carried out using an Agilent 1260 Infinity II LC/MSD XT system (Amstelveen, The Netherlands). Electrospray ionization in positive mode was used to confirm the identity of the synthesized products. Purifications were performed on a preparative high-performance liquid chromatography (HPLC) using an Agilent 1290 Infinity II system equipped with an autosampler and a fraction collector. UV absorbance was measured at 230, 254, and 280 nm. Both LC systems were controlled by Agilent OpenLab CDS ChemStation software.

5.1.2 Radiochemistry

[^{111}In]$InCl_3$ was provided by Curium (Petten, The Netherlands) and [^{177}Lu]$LuCl_3$ was purchased from PI Medical (Raamdonksveer, The Netherlands). Radio-HPLC analyses were carried out using a Waters 2695 system equipped with a Waters 2998 diode array detector and a radioactivity detector from Canberra (Zadik, Belgium). This HPLC system was controlled by Empower 3 software. Instant thin-layer chromatography (iTLC) was performed on iTLC-SG plates from Agilent (Folsom, CA, USA), eluted with a sodium citrate solution (0.1 M, pH 5.0) and analyzed using a Brightspec bSCAN radio-chromatography scanner (Antwerp, Belgium). Radiochemical yield (RCY) was determined from iTLC, while radiochemical purity (RCP) of the labeled compounds was measured by radio-HPLC. Radioactivity measurements were performed using a VDC-405 dose calibrator from Comecer (Joure, The Netherlands). Radioactive samples for $LogD_{7.4}$ determination, *in vitro* assays, and *in vivo* tissue uptakes were counted using a Wizard 2480 γ-counter from Perkin Elmer (Waltham, MA, USA) or a Hidex AMG automatic gamma counter (Turku, Finland).

5.2 HPLC conditions

The LC-MS analyses were performed on an Agilent Poroshell 120 EC-C18 column (3 x 100 mm, 2.7 µm) at a flow rate of 0.5 mL/min and with a mobile phase consisting of: A [0.1% formic acid (FA) in water, *v/v*] and B [0.1% FA in acetonitrile (ACN), *v/v*]. Elution of the products was performed according to the following gradient: 0–5 min (5–100% B) and 5–8 min (100% B).

Purification of the dimers was performed using an Agilent Prep C18 column (50 x 21.2 mm, 5 µm). The mobile phase consisted of solvents C [0.1% trifluoroacetic acid (TFA) in water, *v/v*] and D [0.1% TFA in ACN, *v/v*] at a flow rate of 10 mL/min. The following elution method was used: 0–2 min (5–20% D), 2–10 min (20–40% D) and 10–12 min (40–100% D).

The analyses of the radioactive products were performed on an analytical Gemini C_{18} column (250.0 x 4.6 mm, 5 µm) from Phenomenex (Torrance, CA, USA) at a flow rate of 1 mL/min. The mobile phase consisted of: E [0.1% TFA in water, *v/v*] and F [0.1% TFA in ACN, *v/v*]. Elution of the products was performed according to the following gradient: 0-3 min (5% F), 3-23 min (5 to 100% F) and 23-27 min (100% F).

5.3 Chemical synthesis

The FAP-targeting building block **9** and the triazine-based platform **5** were synthesized according to procedures previously reported by our group (46). Detailed synthetic procedures of the SSTR2-targeting peptide, homodimer **8**, and SSTR2-FAP heterodimer **14**, as well as chromatograms and spectrometric analyses, are provided in the Supplementary Materials (Figures S1-S10).

5.4 Binding affinity

All enzymatic assays were performed in black 384-well plates (Corning, high-binding, flat-bottom), and enzymatic activity was measured at λ_{EX} 350 nm/λ_{EM} 485 nm on a Hidex Sense microplate reader (Turku, Finland). For huFAP and muFAP assay, 50 µL of reaction mixture consisting of 10 µM Z-Gly-Pro-AMC substrate (Abcam; Cambridge, UK), 10 ng huFAP or muFAP protein (Biolegend; San Diego, CA, USA), and assay buffer (50 mM Tris, 100 mM NaCl, and 1.5 µM BSA, DMSO (1% v/v), pH 7.4), were supplemented with increasing concentrations (10^{-11} M to 10^{-5} M) of SSTR2-FAP heterodimer **14** or FAPI-46. Val-boroPro (10^{-4} M) from Bachem (Bubendorf, Switzerland) and assay buffer served as positive and negative controls, respectively. The enzymatic assay of DPP4 contained 100 µM of H-Gly-Pro-AMC substrate (MedChemExpress; Monmouth Junction, NJ, USA), 10 nM DPP4 (Abcam; Cambridge, UK), assay buffer and increasing concentrations (10^{-10} M to 10^{-4}M) of **14**. Sitagliptin (10^{-4} M) from Abcam and assay buffer were used as positive and negative controls, respectively. H-Gly-Pro-AMC in assay buffer was used as a baseline control. The plates were analyzed by microplate reader at 37 °C under dark conditions after 1 h (huFAP), 2 h (muFAP), or 30 min (DPP4). For all assays, the components were kept on ice before plating and experiments were performed in triplicate.

5.5 Radiolabeling

Prior to labeling, the concentrations of the dimers were determined by titration according to a method previously described (47). [^{111}In]$InCl_3$ or [^{177}Lu]$LuCl_3$ in 0.5 M HCl was added to a mixture of FAPI-46, DOTA-TATE or dimers (**8**, **14**), ascorbic acid/gentisic acid (10 µL, 50 mM), ethanol (10 µL), sodium acetate (1 µL, 2.5 M), and H_2O (final volume of 140 µL). For *in vitro* studies, [^{177}Lu]Lu-labeled compounds (DOTA-TATE, FAPI-46, and dimers **8** and **14**) were prepared at a molar activity of 20 MBq/nmol and used for cell uptake and receptor binding

assays. *In vitro* autoradiography was performed using [^{111}In]In-FAPI-46 at a molar activity of 20 MBq/nmol. For *ex vivo* biodistribution studies, [^{177}Lu]Lu-labeled dimers (**8** and **14**) were administered at a molar activity of 5 MBq/nmol. The mixture was incubated for 15 min at 90 °C. To complex any remaining free radionuclide, 5 µL of diethylenetriaminepentaacetic acid (DTPA) at a concentration of 3 mg/mL was added.

5.6 *In vitro* stability

[^{177}Lu]Lu-**8** or [^{177}Lu]Lu-**14** (~3 MBq) was incubated in 300 µL of PBS (0.1 M, pH 7.4) or murine serum at 37 °C. The stability of the radiolabeled peptide was assessed at 1, 4, and 24 h post-incubation. No prior treatment was required for the samples in PBS before analysis by radio-HPLC. However, an equal volume of acetonitrile was added to the samples in murine serum to precipitate the proteins. The solution was then centrifuged for 10 min at 13'000 rpm, and the supernatant was subsequently subjected to radio-HPLC analyses.

5.7 $LogD_{7.4}$

Distribution coefficients ($LogD_{7.4}$) were determined using the shake-flask method. A sample containing [^{177}Lu]Lu-**8** or [^{177}Lu]Lu-**14** (~ 0.5 MBq) was added to 500 µL of PBS (pH 7.4) and 500 µL of *n*-octanol. The vial was vigorously vortexed and then centrifuged at 10'000 rpm for 10 min to allow phase separation. Samples of 10 µL from both phases were collected and measured in the γ-counter. Measurements were performed in triplicates and the $LogD_{7.4}$ value was calculated using the following equation: $LogD_{7.4}$ = log [(counts in n-octanol phase)/(counts in aqueous phase)].

5.8 Cell culture

Human osteosarcoma cells (U2OS) transfected with SSTR2 receptor (U2OS.SSTR2) and the human sarcoma HT-1080 and HT-1080.huFAP cell lines were cultured in DMEM Glutamax© (Gibco; Breda, The Netherlands) supplemented with 2 mM L-glutamine, 10% FBS, 50 UI/mL penicillin, and 50 µg/mL streptomycin. NCI-H69 cells from ATCC (Manassas, VA, USA) were cultured in Gibco™ RPMI 1640 Medium supplemented with 2 mM glutamine (Fisher Scientific; Landsmeer, The Netherlands), penicillin (50 units/mL), streptomycin (50 µg/mL) and 10% fetal bovine serum (FBS). All cell lines were regularly passaged at 80% confluence and maintained at 37 °C and 5% CO_2.

5.9 Uptake/internalization studies

U2OS.SSTR2 cells were seeded in 6-well plates 24 hours before the experiment (5×10^5 cells/well). HT-1080.huFAP cells were seeded in 12-well plates 24 hours before the experiment (1×10^5 cells/well). Adhered cells were incubated with 10^{-9} M of [^{177}Lu]Lu-DOTA-TATE, [^{177}Lu]Lu-FAPI-46, [^{177}Lu]Lu-**8** or [^{177}Lu]Lu-**14** in 1 mL or 750 µL (for U2OS.SSTR2 or HT-1080.huFAP, respectively) of internalization medium (RPMI medium supplemented with 2 mM glutamine, 20 mM HEPES, and 1% BSA w/v, pH 7.4) for 0.5, 1, or 2 h at 37 °C and 5% CO_2. Uptake specificity was evaluated with a block containing 1000-fold excess of non-labelled DOTA-TATE or FAPI-46. After incubation, medium was removed and cells were washed twice

with cold PBS. The membrane-bound fraction was collected by incubating cells with an acid buffer (50 mM glycine, 100 mM sodium chloride, pH 2.8) for 10 min at room temperature (rt). Cells were lysed using sodium hydroxide (1 M) for 5 min at rt to obtain the internalized fraction. Both fractions were measured in the γ-counter. Data were analyzed in GraphPad Prism 9.0 and expressed as percentage of added dose.

5.10 Binding affinity assay

U2OS.SSTR2 cells were seeded in a 24-well plate 24 h prior to the assay (1×10^5 cells/well). Medium was removed and the cells were washed once with PBS. Then, medium (DMEM medium supplemented with 2 mM, 20 mM HEPES, and 1% BSA, pH 7.4) containing [^{177}Lu]Lu-DOTA-TATE (10^{-9} M) and decreasing concentrations of unlabeled **8**, **14**, or DOTA-TATE (10^{-13} to 10^{-6} M) were added. Cells were incubated at 37 °C for 90 min. After incubation, the medium was removed, and cells were washed twice with cold PBS and lysed with 1 M NaOH for 5 min at rt. The lysate was transferred to counting tubes, and measurement was performed using the γ-counter. For each concentration, experiments were performed in triplicate. The 50% inhibition constant (IC_{50}) was calculated by fitting the data to a one-site Fit-Ki curve in GraphPad Prism v9.

5.11 Animal models

Six-week-old female Balb/c nu/nu-specific mice (Janvier; Le Genest-Saint-Isle, France) were housed in individually ventilated cages (4 mice/cage). Upon arrival, mice were acclimated for one week, with access to food and water ad libitum. Mice were subcutaneously inoculated on the right shoulder with NCI-H69 cells (5×10^6 cells) suspended in 100 µL of 1/3 Matrigel (Corning Inc.; Corning, NY, USA) and 2/3 Hank's balanced salt solution (Gibco; Paisley, UK). NCI-H69 xenografts were allowed to grow for 2 weeks, reaching a tumor size over 200 mm^3 at the start of the study.

5.12 *Ex Vivo* Biodistribution

To determine the biodistribution of the compounds, mice were intravenously injected with 100 µL of radiotracer. At specific time points (1, 4, and 24 h post-injection), blood was collected via retro-orbital puncture under isoflurane/O_2 anesthesia, after which the mice were sacrificed via cervical dislocation. Tumors and organs of interest (heart, lungs, liver, spleen, stomach, large and small intestine, pancreas, kidneys, muscle, skin, and bone) were excised, washed in PBS, blotted dry, and collected into tubes. All collected tissues were weighed and measured in the γ-counter. The percentage of injected dose per gram (% ID/g) was determined for each tissue sample and corrected for the injected activity and the % ID present at the injection site.

5.13 Autoradiography studies

In vitro autoradiography studies were conducted using fresh-frozen NCI-H69 and HT-1080.huFAP tumor xenografts. Fresh-frozen NCI-H69 and HT1080.huFAP tumors were cryosectioned into 10 µm slices and mounted on Starfrost PlusTM microscope slides (VWR, Leuven, Belgium) using the CryoStar NX70 cryostat (Thermo Scientific, Waltham, MA, USA).

Autoradiographic binding studies were performed as previously described (48). First, tissue slices were pre-incubated for 10 min at rt in washing buffer containing 167 mM Tris-HCl, pH 7.6, 5 mM $MgCl_2$ and 0.25% BSA. Sections were then incubated for 1 h at rt with 100 µL of 10^{-9} M [^{111}In]In-FAPI-46. Binding specificity was assessed on adjacent sections by co-incubation with 10^{-6} M unlabeled FAPI-46. After incubation, the slides were washed three times with cold buffer and air-dried prior to imaging. All autoradiographic images were acquired using the BeaQuant imaging system (Atlantic Instruments for Research, Nantes, France) and analyzed using Beamage software version 3.1.1 (Atlantic Instruments for Research). Radiotracer binding was expressed as % AA measured in counts/mm^2/min. Tumor sections were subsequently subjected to hematoxylin and eosin (H&E) staining.

5.14 FAP-specific immunohistochemistry (IHC)

FAP expression in fresh-frozen NCI-H69 and HT-1080.huFAP xenograft tissues was evaluated by automated chromogenic immunohistochemistry using a Ventana BenchMark Discovery ULTRA system (Ventana Medical Systems Inc.). Immediately after excision, xenograft tumors were embedded in Cryo-Gel in tin cans and snap-frozen in liquid nitrogen. On the day of staining, the tumors were sectioned at a thickness of 4 µm using a CryoStar NX70 cryostat (Thermo Scientific, Waltham, MA, USA). Sections were mounted on Superfrost Plus™ microscope slides (VWR, Leuven, Belgium), air-dried, and fixed in ice-cold acetone for 10 min at -20°C. The sections were subsequently incubated with the rabbit monoclonal anti-FAP antibody EPR20021 (Abcam, Cambridge, UK) at a 1:50 dilution for 32 min at 37°C. Antibody binding was detected using the OmniMap anti-rabbit HRP reagent (cat. no. 760-4311, Ventana), followed by chromogenic development with the ChromaMap DAB Detection Kit (cat. no. 760-159, Ventana). Sections were counterstained with Hematoxylin II and treated with blue reagent according to the manufacturer's instructions.

5.15 Statistics

All statistical analyses were performed with GraphPad Prism version 9.0 (San Diego, CA, USA). IC_{50} values and curves were determined using a non-linear regression Log(inhibitor) vs. response analysis with variable slope (four-parameters). Tumor and organ clearance graphs were calculated by one-phase decay linear regression, corrected for the grow-in phase when applicable. Data are reported as mean ± SD (standard deviation) for at least three independent replicates. Unpaired two-tailed Student's t-tests were used for group comparisons.

Declarations

Ethics approval and consent to participate: The study was conducted according to the guidelines of the Declaration of Helsinki. Approval was granted by the Animal Welfare Committee of the Erasmus MC (CCD#: 2216075, SP2400006; CCD#: 2216075, SP2200175).

Consent for publication: Not applicable.

Availability of data and material: All available data are described in the manuscript and available through the supplementary material. Additional information can be obtained by contacting the authors upon reasonable request.

Competing interests: The authors declare that they have no competing interests.

Funding: Le Li was supported by the China Scholarship Council (CSC).

Author Contributions: Le Li (L.L.) and Hanyue Ma (H.M.) contributed equally to this work. L.L. contributed to investigation, formal analysis, and writing-review & editing. H.M. contributed to investigation and writing-review & editing. Dylan Blijleven (D.B.) contributed to investigation, validation and formal analysis. Amber Piet (A.P.) contributed to investigation, software, validation, formal analysis, and writing-review & editing. Corrina de Ridder (C.R.) contributed to investigation and writing-review & editing. Debra Stuurman (D.S.) contributed to investigation and writing-review & editing. Priciana Paraïso (P.P.) contributed to software, validation, formal analysis, and writing-review & editing. Yann Seimbille (Y.S.) contributed to conceptualization, methodology, supervision, project administration, funding acquisition, and writing-review & editing. All authors read and approved the final manuscript.

Acknowledgement: The human sarcoma HT-1080.huFAP cell line, stably transduced with human FAP, was kindly provided by Uwe Haberkorn (University of Heidelberg), Christoph Renner (KHO) and Stefan Bauer (NCT Heidelberg). The authors gratefully acknowledge technical and financial support from the Erasmus Medical Center.

6 References

1. Fernandez-Cuesta L, Alcala N, Mathian E, Derks J, Thirlwell C, Dayton T, et al. Basic science and translational implications of current knowledge on neuroendocrine tumors. J Clin Invest. 2025;135(5):e186702.
2. Di Franco M, Zanoni L, Fortunati E, Fanti S, Ambrosini V. Radionuclide Theranostics in Neuroendocrine Neoplasms: An Update. Curr Oncol Rep. 2024;26(5):538-50.
3. Pedraza-Arevalo S, Gahete MD, Alors-Perez E, Luque RM, Castano JP. Multilayered heterogeneity as an intrinsic hallmark of neuroendocrine tumors. Rev Endocr Metab Disord. 2018;19(2):179-92.
4. Iravani A, Parihar AS, Akhurst T, Hicks RJ. Molecular imaging phenotyping for selecting and monitoring radioligand therapy of neuroendocrine neoplasms. Cancer Imaging. 2022;22(1):25.
5. Vijayvergia N, Lee LS, Katona BW. Gastroenteropancreatic Neuroendocrine Tumors. Gastroenterology. 2026;170(1):34-49.
6. Hernandez-Felix JH, Meneses-Medina MI, Riechelmann R, Strosberg J, Garcia-Carbonero R, Rivero JD. Emerging Diagnostics and Therapies in Neuroendocrine Neoplasms: A Critical Review. Cancers (Basel). 2025;17(22):3632.
7. Sedlack AJH, Varghese DG, Naimian A, Yazdian Anari P, Bodei L, Hallet J, et al. Update in the management of gastroenteropancreatic neuroendocrine tumors. Cancer. 2024;130(18):3090-105.

8. Liberini V, Huellner MW, Grimaldi S, Finessi M, Thuillier P, Muni A, et al. The Challenge of Evaluating Response to Peptide Receptor Radionuclide Therapy in Gastroenteropancreatic Neuroendocrine Tumors: The Present and the Future. Diagnostics (Basel). 2020;10(12):1083.
9. Santoro-Fernandes V, Schott B, Weisman AJ, Lokre O, Cho SY, Perlman SB, et al. Full-Body Tumor Response Heterogeneity of Metastatic Neuroendocrine Tumor Patients Undergoing Peptide Receptor Radiopharmaceutical Therapy. J Nucl Med. 2025;66(4):565-71.
10. Haugh KN, Sanwick AM, Chaple IF. Targeted radionuclide therapy and diagnostic imaging of SSTR positive neuroendocrine tumors: a clinical update in the new decade. Front Nucl Med. 2025;5:1655419.
11. Hope TA, Bodei L, Chan JA, El-Haddad G, Fidelman N, Kunz PL, et al. NANETS/SNMMI Consensus Statement on Patient Selection and Appropriate Use of (177)Lu-DOTATATE Peptide Receptor Radionuclide Therapy. J Nucl Med. 2020;61(2):222-7.
12. Ambrosini V, Zanoni L, Filice A, Lamberti G, Argalia G, Fortunati E, et al. Radiolabeled Somatostatin Analogues for Diagnosis and Treatment of Neuroendocrine Tumors. Cancers (Basel). 2022;14(4):1055.
13. Vahidfar N, Farzanehfar S, Abbasi M, Mirzaei S, Delpassand ES, Abbaspour F, et al. Diagnostic Value of Radiolabelled Somatostatin Analogues for Neuroendocrine Tumour Diagnosis: The Benefits and Drawbacks of [(64)Cu]Cu-DOTA-TOC. Cancers (Basel). 2022;14(8):1914.
14. Fonti R, Panico M, Pellegrino S, Pulcrano A, Vastarella LA, Torbati AHM, et al. Heterogeneity of SSTR2 Expression Assessed by (68)Ga-DOTATOC PET/CT Using Coefficient of Variation in Patients with Neuroendocrine Tumors. J Nucl Med. 2022;63(10):1509-14.
15. Karimi A, Bogdani C, O'Dwyer E, Siolas D. Emerging innovations in theranostics for pancreatic neuroendocrine tumors. NPJ Precis Oncol. 2025;9(1):146.
16. Zhang S, Sun X, Liu W, Wu J, Wu Y, Jiang S, et al. Determining the Multivalent Effects of d-Peptide-Based Radiotracers. Chem Biomed Imaging. 2025;3(3):180-90.
17. Jin W, Yan L, Li L, Luo Y, Qiao J, Peng Q, et al. PSMA and SSTR2 Dual-Targeting Theranostic Agents for Neuroendocrine-Differentiated Prostate Cancer (NEPC). J Med Chem. 2025;68(2):1984-93.
18. Judmann B, Braun D, Wangler B, Schirrmacher R, Fricker G, Wangler C. Current State of Radiolabeled Heterobivalent Peptidic Ligands in Tumor Imaging and Therapy. Pharmaceuticals (Basel). 2020;13(8):173.
19. Liu H, Zhang X, Pan Y, Zhang J, Wen H, Zhang C, et al. Preclinical Study of a Dual-Target Molecular Probe Labeled with (68)Ga Targeting SSTR2 and FAP. Pharmaceuticals (Basel). 2024;17(12):1647.
20. Lee HH, Al-Ogaili Z. Fibroblast activation protein and the tumour microenvironment: challenges and therapeutic opportunities. Oncol Rev. 2025;19:1617487.
21. Vlachostergios PJ, Karathanasis A, Tzortzis V. Expression of Fibroblast Activation Protein Is Enriched in Neuroendocrine Prostate Cancer and Predicts Worse Survival. Genes (Basel). 2022;13(1):135.
22. Fouillet J, Torchio J, Rubira L, Fersing C. Unveiling the Tumor Microenvironment Through Fibroblast Activation Protein Targeting in Diagnostic Nuclear Medicine: A Didactic Review on Biological Rationales and Key Imaging Agents. Biology (Basel). 2024;13(12):967.

23. Prive BM, Boussihmad MA, Timmermans B, van Gemert WA, Peters SMB, Derks YHW, et al. Fibroblast activation protein-targeted radionuclide therapy: background, opportunities, and challenges of first (pre)clinical studies. Eur J Nucl Med Mol Imaging. 2023;50(7):1906-18.
24. Loktev A, Lindner T, Burger EM, Altmann A, Giesel F, Kratochwil C, et al. Development of Fibroblast Activation Protein-Targeted Radiotracers with Improved Tumor Retention. J Nucl Med. 2019;60(10):1421-9.
25. Backhaus P, Gierse F, Burg MC, Buther F, Asmus I, Dorten P, et al. Translational imaging of the fibroblast activation protein (FAP) using the new ligand [(68)Ga]Ga-OncoFAP-DOTAGA. Eur J Nucl Med Mol Imaging. 2022;49(6):1822-32.
26. Chapeau D, Koustoulidou S, Handula M, Beekman S, de Ridder C, Stuurman D, et al. [(212)Pb]Pb-eSOMA-01: A Promising Radioligand for Targeted Alpha Therapy of Neuroendocrine Tumors. Pharmaceuticals (Basel). 2023;16(7):985.
27. Ma H, Li L, Piet A, Handula M, de Ridder C, Stuurman D, et al. A new series of FAP inhibitors for cancer imaging based on 8-substituted (4-quinolinoyl)-glycyl-2-cyanopyrrolidine. Nucl Med Biol. 2026;158-159:109661.
28. Li L, Ma H, Piet A, de Ridder C, Stuurman D, Paraïso P, et al. eFAP-51, a novel FAPI dimer with enhanced tumor uptake and retention for theranostic applications. Ejnmmi Radiopharm Ch. 2026.
29. Zhao L, Pang Y, Fang J, Chen J, Zhou Y, Sun L, et al. Design, Preclinical Evaluation, and Clinical Translation of (68)Ga-FAPI-LM3, a Heterobivalent Molecule for PET Imaging of Nasopharyngeal Carcinoma. J Nucl Med. 2024;65(3):394-401.
30. Dupire C, Chennell P, Pereira B, Courtiol N, Buj S, Cueff R, et al. A proof of principle study using radiopharmaceuticals to quantify and localize container-content interactions in medical syringes. Sci Rep. 2023;13(1):2721.
31. Dean TT, Jelu-Reyes J, Allen AC, Moore TW. Peptide-Drug Conjugates: An Emerging Direction for the Next Generation of Peptide Therapeutics. J Med Chem. 2024;67(3):1641-61.
32. Wang D, Yin F, Li Z, Zhang Y, Shi C. Current progress and remaining challenges of peptide-drug conjugates (PDCs): next generation of antibody-drug conjugates (ADCs)? J Nanobiotechnology. 2025;23(1):305.
33. Chapeau D, Beekman S, Handula M, Murce E, de Ridder C, Stuurman D, et al. eTFC-01: a dual-labeled chelate-bridged tracer for SSTR2-positive tumors. EJNMMI Radiopharm Chem. 2024;9(1):985.
34. Dobitz S, Wilhelm P, Romantini N, De Foresta M, Walther C, Ritler A, et al. Distance-Dependent Cellular Uptake of Oligoproline-Based Homobivalent Ligands Targeting GPCRs-An Experimental and Computational Analysis. Bioconjug Chem. 2020;31(10):2431-8.
35. Gervasoni S, Guccione C, Fanti V, Bosin A, Cappellini G, Golosio B, et al. Molecular simulations of SSTR2 dynamics and interaction with ligands. Sci Rep. 2023;13(1):4768.
36. Qu YA, Huang JC, Wang ZV, Ferguson AL, Nguyen JMH, Zhang M, et al. Understanding the Cancer-Associated Fibroblast (CAF) and Its Biomarker Fibroblast Activation Protein (FAP), and Aspects in Human Liver Cancer. Front Biosci (Landmark Ed). 2025;30(12):44837.
37. Linxweiler J, Hajili T, Korbel C, Berchem C, Zeuschner P, Muller A, et al. Cancer-associated fibroblasts stimulate primary tumor growth and metastatic spread in an orthotopic prostate cancer xenograft model. Sci Rep. 2020;10(1):12575.

38. Ma Y, Lin Z, Fallon JK, Zhao Q, Liu D, Wang Y, et al. New mouse xenograft model modulated by tumor-associated fibroblasts for human multi-drug resistance in cancer. Oncol Rep. 2015;34(5):2699-705.
39. Geenen L, Nonnekens J, Konijnenberg M, Baatout S, De Jong M, Aerts A. Overcoming nephrotoxicity in peptide receptor radionuclide therapy using [(177)Lu]Lu-DOTA-TATE for the treatment of neuroendocrine tumours. Nucl Med Biol. 2021;102-103:1-11.
40. Walrand S, Jamar F. Renal and Red Marrow Dosimetry in Peptide Receptor Radionuclide Therapy: 20 Years of History and Ahead. Int J Mol Sci. 2021;22(15):8326.
41. Sobral MC, Mota SI, Oliveira PJ, Urbano AM, Paulo A. Two Targets, One Mission: Heterobivalent Metal-Based Radiopharmaceuticals for Prostate Cancer Imaging and Therapy. ChemMedChem. 2025;20(11):e202500128.
42. Lanzafame H, Mavroeidi IA, Pabst KM, Desaulniers M, Ingenwerth M, Hirmas N, et al. (68)Ga-Fibroblast Activation Protein Inhibitor PET/CT Improves Detection of Intermediate and Low-Grade Sarcomas and Identifies Candidates for Radiopharmaceutical Therapy. J Nucl Med. 2024;65(6):880-7.
43. Kalantari F, Hormann AA, Pokarowski M, Kalantari E, Jung TE, Schweighofer-Zwink G, et al. Fibroblast Activation Protein Inhibitor (FAPI)-Radioligand PET/CT in the Assessment of Nononcological Diseases: A Narrative Review. Acs Pharmacol Transl. 2025;8(12):4193-213.
44. Gundogan C, Guzel Y, Can C, Kaplan I, Komek H. FAPI-04 Uptake in Healthy Tissues of Cancer Patients in (68)Ga-FAPI-04 PET/CT Imaging. Contrast Media Mol Imaging. 2021;2021:9750080.
45. Bentestuen M, Al-Obaydi N, Zacho HD. FAPI-avid nonmalignant PET/CT findings: An expedited systematic review. Semin Nucl Med. 2023;53(5):694-705.
46. Ma H, de Muynck L, Houvast RD, Beekman S, Piet A, March TL, et al. Revolutionizing Solid Tumor Surgery with Fibroblast Activation Protein (FAP)-Targeted Imaging Probes for a Fluorescence-Guided Surgery of Pancreatic Cancer. Bioconjug Chem. 2025;36(10):2145-57.
47. Breeman WAP, Chan HS, de Blois E. Determination of peptide content and purity of DOTA-peptides by metal ion titration and UPLC: an alternative method to monitor quality of DOTA-peptides. J Radioanal Nucl Chem. 2014;302(2):825-30.
48. Damiana TST, Paraiso P, de Ridder C, Stuurman D, Seimbille Y, Dalm SU. Side-by-side comparison of the two widely studied GRPR radiotracers, radiolabeled NeoB and RM2, in a preclinical setting. Eur J Nucl Med Mol Imaging. 2023;50(13):3851-61.

Supplementary Files

This is a list of supplementary files associated with this preprint. Click to download.

- SISSTR2dimersfinal.docx